Collective Dynamics

Effect of Response Time Distribution in Weak Lane Discipline on Linear Stability

Akihito Nagahama[1] · **Akiyasu Tomoeda**[2] · **Takahiro Wada**[3]

[1] The University of Electro-Communications, Tokyo, Japan,
E-mail: naga0862@uec.ac.jp
[2] Kansai University, Osaka, Japan,
E-mail: tomoeda@kansai-u.ac.jp
[3] Nara Institute of Science and Technology, Nara, Japan,
E-mail: t.wada@is.naist.jp

Received: 26 September 2024 / Last revision received: 17 April 2025 / Accepted: 17 April 2025
DOI: 10.17815/CD.2025.188

Abstract The increase in mixed traffic with weak lane discipline (2D mixed traffic) has attracted significant research attention. To better replicate and understand traffic with weak lane discipline, this study examined the variation in response time relative to the position of the leading vehicle, including lateral shifts. Through experiments conducted using a driving simulator and functional fitting, we demonstrated that changes in response time due to longitudinal and lateral locational shifts are well represented by linear and exponential functions, respectively. Additionally, we proposed an extended formulation of the 2D optimal velocity model (2D OVM) that incorporates variable response times, termed the 2D OVM with varying sensitivities (2D OVMVS). The stability condition was derived using a linear approximation. A comparative analysis of the phase diagrams of the 2D OVM and 2D OVMVS, along with a sensitivity analysis, revealed that the proposed 2D OVMVS exhibited a larger unstable region in the phase diagram and lower stability in stable regions than the 2D OVM. As a result, in 2D traffic with weak lane discipline, the equilibrium formation of vehicles was more susceptible to disruption. Our findings indicate that variable response times, as observed in this study, substantially influence the stability of no-lane traffic. Unlike fixed-response models, incorporating response time variability accentuates unstable tendencies. This underscores the necessity of accounting for non-uniform response time distributions in future traffic models.

Keywords Traffic flow · weak lane discipline · response time · stability

1. Introduction

Vehicular traffic congestion has become a critical issue in both developing and developed countries, contributing to increased travel times, energy waste, elevated pollution levels, and adverse health effects [1–3]. As highlighted in previous studies [4–10], vehicular traffic in developing countries exhibits distinct characteristics that differ from those observed in developed countries. In general, vehicular traffic can be classified based on the intensity of lane discipline and the heterogeneity of vehicle types, as illustrated in Fig. 1. Traffic observed in many developing countries is categorized as two-dimensional (2D) mixed traffic in Fig. 1 because it typically consists of various vehicle types with weak lane discipline. In 2D traffic, vehicle interactions occur in multiple directions more intensively than in one-dimensional (1D) traffic, where lane discipline is more strictly maintained. Consequently , speed disturbances that trigger congestion can propagate and amplify in multiple directions. This characteristic underscores the importance of incorporating such dynamics into mathematical analyses and replication models for 2D traffic.

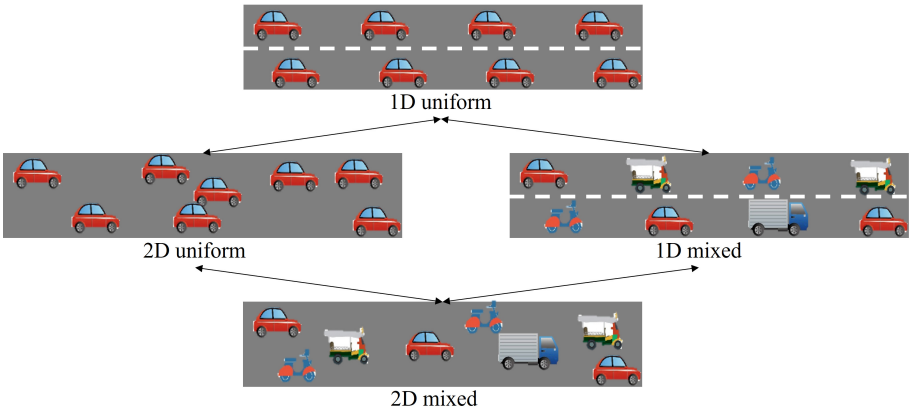

Figure 1 Classification of traffic by lane discipline intensity and heterogeneity of vehicle type.

Stability is a key indicator of whether velocity disturbances, which contribute to congestion, will amplify over time. A traffic condition is considered (linearly) stable when vehicle velocities remain synchronized, and any small velocity disturbance affecting certain vehicles is attenuated as it propagates to following vehicles, preventing congestion caused by such disturbances. Therefore, the stability condition—satisfied by stable traffic but not by unstable traffic—is essential for understanding traffic characteristics and dynamics. As foundational studies on the stability of 2D mixed traffic, research has focused on mathematical models [11, 12] to replicate the diverse behaviors of various vehicle types, such as speeds, accelerations, and headways [13–16]. Additionally, studies have explored the stability of one-dimensional (1D), i.e., lane-based, mixed traffic [17–20]. These studies [17–20] have successfully demonstrated that the stability condition varies based on the composition ratio of vehicle types in traffic and the sequence of leader-follower vehicle pairs. However, these studies assumed lane-based traffic without considering overtaking maneuvers or the relative lateral positions of vehicles.

Attempts have also been made to theoretically investigate the stability of 2D mixed traffic using the lattice hydrodynamics (LH) model [21]. Mohan et al. extended the LH model to incorporate overtaking in 2D mixed traffic [22], while Chattopadhyay et al. applied this model to compute statistical indices for assessing regime shifts in traffic flow and analyzing linear stability [23]. The LH model computes the density, speed, and flow of each vehicle type at a macroscopic level based on the continuity equation. In contrast, microscopic models, such as car-following models, determine driver acceleration individually based on vehicle velocity, the distance to surrounding vehicles, and velocity differences. Microscopic models explicitly represent the behavior of individual drivers and vehicle types, which have been extensively studied in prior research [13–16]. By simulating the behavior of a single vehicle, these models reproduce overall traffic flow. Thus , microscopic models are more suitable than the LH model for applications requiring precise modeling of driver behavior and individual vehicle interactions to assess their effects on traffic flow.

In fact, several studies have investigated 2D traffic using microscopic models. For instance, various models for lateral vehicle maneuvering have been proposed to replicate lateral movements distinct from lane-based 1D traffic [24–27]. Oketch applied fuzzy logic—a computational approach designed to handle approximate reasoning—to represent the arbitrary yet discrete lateral positions of vehicles. Furthermore, by utilizing traffic data from Nairobi, Kenya, he successfully derived parameters for microscopic models describing both longitudinal and lateral vehicle behavior [28]. Kanagaraj et al. developed a 2D vehicular model and estimated its parameters [29]. In their model, lateral behavior was represented using continuous equations rather than discrete ones. These studies have primarily focused on reproducing traffic through simulation but have not yet explored stability considerations within microscopic models. Beyond simulation studies, it is essential to gain insights through theoretical approaches, such as the theoretical derivation of stability conditions, to examine how the detailed behavior of individual vehicles and drivers influences overall traffic flow in 2D mixed traffic. Such theoretical insights offer the advantage of enhancing the efficiency of simulation studies by validating their results and providing a broader perspective on parameter selection.

For example, the theoretical stability of two-lane traffic has been investigated while considering factors such as heterogeneity [30], horn effects [31], and V2V communication technology [32]. In these studies, models resembling 2D traffic are employed, where vehicle acceleration and deceleration are influenced by neighboring vehicles with lateral deviations in adjacent lanes. However, these studies still assume the presence of lanes or imaginary lane structures and do not fully capture the characteristics of 2D traffic, where velocity disturbances propagate in multiple directions.

As an example of a model and stability analysis in which disturbances can propagate in all directions without any lane-based assumptions, Nakayama's 2D Optimal Velocity Model (OVM) [33] and the microscopic model for lane-less traffic [34] can be referenced. However, it is important to note that the aforementioned microscopic models, including the 2D OVM, have only considered variations in the intensity of driver reactions to lateral displacement in 2D traffic. Based on previous perception and psychological experiments [35, 36], it is reasonable to assume that lateral displacement influences not only the

intensity of reactions but also drivers' response times. To summarize the discussion so far, to the best of our knowledge, the following evaluations have not yet been conducted:

- Whether response time varies with the position of the leading vehicle, and, if so, a quantitative measurement of such changes.
- The assessment of its impact on the stability of 2D traffic.

When comparing Nakayama's 2D OVM [33] and the microscopic model for lane-less traffic [34], including the 2D OVM, OVMs can incorporate a sensitivity parameter that essentially represents the time duration required for speed adjustment. This adjustment duration accounts for both the time drivers take to respond to the acceleration or deceleration of leading vehicles and the time required to operate their pedals. If response time varies with changes in the repulsive force based on lateral and longitudinal positions, such variations in adjustment duration can be integrated into the sensitivity parameter, representing the overall time required for speed adjustment, including response time.

Therefore, this study aimed to measure response times for both lateral and longitudinal displacements through a subject experiment using a driving simulator and integrate these response times into the adjustment duration in the 2D OVM to assess their impact on stability. Depending on the distribution of response times, it is possible to identify unstable traffic conditions that cannot be predicted solely based on changes in reaction intensity considered in previous studies. To clarify the effect of response time variations on the stability of the assumed 2D traffic, this study compared the stability results obtained from experiments with both the traditional model[33] and the newly proposed 2D OVM.

Through our investigation, we aim to achieve the following:

- Gain insights into how the conditions and rate at which velocity disturbances develop in actual 2D traffic deviate from models that do not account for response time.
- Observe the potential impact of response time on behaviors specific to 2D vehicle platooning.

The remainder of this paper is structured as follows:

- We analyze response times for various lateral displacements using a driving simulator (Section 2).
- To incorporate the observed response variations into the 2D OVM, we fit a function between relative position and the measured response time, selecting the model equation based on the observed data (Section 3).
- Meanwhile , we extend the 2D OVM by modifying its sensitivity to integrate the observed response time and derive the stability index of the extended model (Section 4).

- Finally, we apply the observed response time to the extended 2D OVM and evaluate its influence on stability by comparing it with Nakayama's phase diagram (Section 5).

Thus, this study highlights the potential for evaluation errors when assessing the stability of 2D traffic without accounting for response time.

2. Experiment to measure the response time

2.1. Experimental equipment

In the experiment, a fixed-base driving simulator (DS) equipped with five monitors was used (refer to Fig. 2). The behavior of the ego vehicle was simulated using Carsim by Mechanical Simulation, while the leader vehicle was controlled using DS-nano- by Advanced Solutions Technology Japan. Both systems operated at a calculation frequency of 10 ms. Additionally, force feedback was implemented for the ego vehicle's steering. A button was mounted on the steering wheel that the driver could press and hold. This button was used to respond to the leader vehicle's deceleration. Further details are provided in Sec. 2.2. To prevent potential influences on the driver's response to the leader vehicle's behavior, background elements such as urban scenery were not depicted, and no additional road environments were included aside from the road and the leader vehicle. Additionally, the speedometer, tachometer, rearview mirror, and side mirrors were displayed on the DS screen.

Figure 2 Driving simulator used in the experiment.

2.2. Experimental method

The experiments described here are based on results previously presented by the authors in [37]. Fig. 3 illustrates the experimental setup. In this setup, two vehicles, a leader (right, colored orange) and a follower (left, colored yellow), traveled at a steady speed of 17 m/s on a straight road. The follower acted as the ego vehicle in the experiment. No other vehicles were present except for the leader and the follower. At the beginning of each trial, the leader's position was randomly selected within the ranges dx_1 to dx_3 and

from dy_1 to dy_3. Both vehicles maintained a constant velocity of 17 m/s in a straight line until the leader began to decelerate. Although subjects held the steering wheel and pedals from the start of the trial, they were not allowed to operate them until the leader initiated deceleration. At the moment the leader started decelerating, its position was ensured to be at the predefined dx, dy coordinates relative to the ego driver. At a random moment, the leader was programmed to abruptly reduce its speed by 5 m/s, resulting in a theoretically infinite deceleration within the simulator. While such a deceleration exceeds what is observed in real vehicles, this configuration was intentionally adopted to provide a clear and consistent stimulus for accurately measuring the subject's reaction time to the leader's deceleration. Then, upon noticing the leader's deceleration, the subject pressed a button. The response time was defined as $\tau = t_{\text{button}} - t_{\text{dec}}$, where t_{button} is the time when the button was pressed, and t_{dec} is the time when the leader began to slow down. After pressing the button, the participant engaged in braking and steering maneuvers to avoid a collision. Prior to the experiment, participants were thoroughly trained on the required actions in response to the leader's sudden braking. Notably, subjects were not permitted to initiate any avoidance maneuvers until after pressing the button.

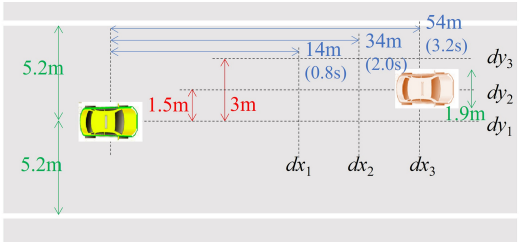

Figure 3 Situation of the experiment and location of the leader.

Fig. 3 illustrates that the experimental road is 10.4 m wide without any lanes. Both the leading and following vehicles are 1.9 m wide. During the experiment, the leader's position relative to the follower was randomly varied across trials. The longitudinal distances (dx) were set at 14 m (dx_1), 34 m (dx_2), and 54 m (dx_3) from the center of the ego vehicle. The figure also displays the corresponding time headways for these distances. The lateral positions (dy) were set at 0 m (dy_1), 1.5 m (dy_2), and 3.0 m (dy_3) to the left of the ego vehicle's center. The setup remained unchanged until the participants detected the leader's deceleration and pressed a button.

Regarding the method for setting dx, we first used the Intelligent Driver Model and its parameters [38] to estimate that a following distance significantly shorter than 36 m at a speed of 17 m/s would result in deceleration exceeding the "comfortable deceleration" defined in [38]. Additionally, applying the two-second rule [39], which is commonly recommended to prevent accidents, yields a time headway of 34 m. Based on this, the intermediate value of dx (dx_2) was set to 34 m, corresponding to a time headway of 2 s. To determine the closest dx_1, the authors conducted repeated trials on the driving simulator. It was observed that with a time headway of 0.8 s, a collision could just barely be avoided within the DS. Therefore, dx_1 was set to 14 m (a headway time of 0.8 s). Lastly, dx_3 was placed equidistant from dx_1 and dx_2, providing additional margin for the time headway.

dy_3 was set wider than the vehicle's width, ensuring that even when the leader decelerates and approaches, it does not collide with the ego vehicle. Conversely, dy_2 was set narrower than the vehicle's width, representing a position where the ego vehicle must respond to avoid a collision despite the lateral offset. Additionally, dy_1, dy_2, and dy_3 were configured to have equal widths.

After familiarizing themselves with the driving simulator (DS), participants were presented with randomized combinations of these positions, experiencing each combination three times. Data on the leader's and follower's positions, along with the timing of button presses, were recorded for each trial.

To account for potential fatigue from the prolonged duration of DS experiments, the study focused on data from one side. This approach ensured that the dataset was sufficiently large for statistical analysis and model fitting while also minimizing the time each participant spent in the experiment.

2.3. Subjects

Thirteen Japanese students took part in the study, as shown in Tab. 1. Their driving frequency varied from once to three times a week to less than once every six months.

Table 1 Information regarding the subjects

Age (year)	Avg. = 22.5, SD = 1.2
Driving experience (year)	Avg. = 2.6, SD = 1.6
Gender	Male = 9, Female = 4

2.4. Results

The results presented in this section and Sec. 3 have already been reported by the authors in [37]. These findings[37] are here as they are essential for analyzing the proposed model introduced in Sec. 4.

Fig. 4 illustrates the measured response times τ based on the leader's positions. Each bar represents the average response time across all subjects. The checkered boxes on the left indicate the average response times for all lateral positions (dy) corresponding to each longitudinal position (dx). Conversely, the outermost yellow boxes display the average values for all longitudinal positions (dx) for each lateral position (dy). Fig. 4(b) and Fig. 4(c) further break down these average response times from Fig. 4(a), with error bars representing the standard deviations.

Initially, a three-way analysis of variance (ANOVA) was performed, considering the longitudinal and lateral positions as well as trial repetitions. Due to the negligible impact of repetitions, potential learning effects were disregarded. The Greenhouse–Geisser correction was applied, and all factors were treated as within-subject factors. Significant differences were observed for both longitudinal and lateral positions; however, their interaction did not reach statistical significance.

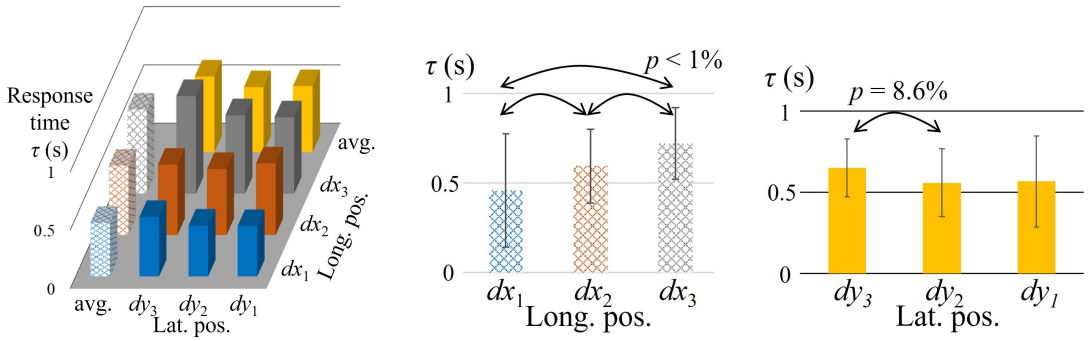

Figure 4 Response time distributions.

3. Function Fitting of the Response Time

We posit that response time is influenced by the combined effects of dx and dy. Given that these effects did not exhibit any maximum or minimum values, we assumed increasing functions for both dx and dy as the fitting functions. The equations presented here serve as candidate models, where dx or dy is represented as q.

$$\tau_q = A_q(q - B_q) + C_q \quad (1)$$
$$\tau_q = A_q \exp(q - B_q) + C_q \quad (2)$$
$$\tau_q = A_q \log(q - B_q) + C_q \quad (3)$$
$$\tau_q = A_q \operatorname{atan}(B_q(q - C_q)) + D_q \quad (4)$$

Tab. 2 presents the top three combinations of functions used to fit the observed response time, ranked by their R^2 values. A linear function and an exponential function were found to be the most suitable for the longitudinal and lateral directions, respectively. Additionally, Tab. 3 lists the fitted parameters of the best-performing functions for each direction. The blue plane depicted in Fig. 5 represents the function fitted to dx and dy. It is reasonable to infer that this function is appropriate, as response time naturally increases with greater longitudinal distance from the leader [40, 41]. Additionally, there is a sharp increase in response time when there is no lateral overlap, specifically when dy exceeds the vehicle width of 1.9 m.

Table 2 Top three fitted functions and their R^2 values.

Rank	Function (longitudinal)	Function (lateral)	R^2
1	linear	exp	0.215
2	atan	atan	0.204
3	linear	linear	0.204

Table 3 Fitted functions and parameters for the response time.

Variable	Response time τ			
R^2	0.215			
Effect	Lateral		Longitudinal	
Function	exp		linear	
Constant	A_{dy} (s)	0.11	A_{dx} (s/m)	0.01
	B_{dy} (m)	2.96	B_{dx} (m)	2.03
	C_{dy} (s)	1.08	C_{dx} (s)	−0.79

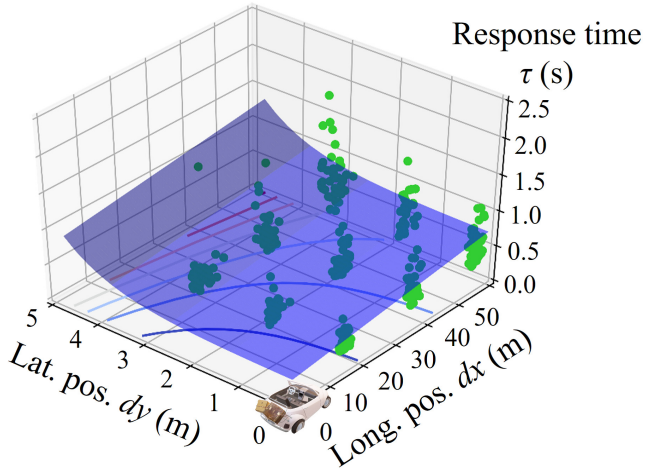

Figure 5 Fitting of the observed response times. The blue surface represents the fitted function, while the green dots correspond to the observed response times. The vehicle depicted in the Figure indicates the position of the ego vehicle.

4. Stability Condition in 2D Traffic Varying the Response Time

4.1. Original 2D OVM and its Stability Condition

In [33], Nakayama et al. configured particles in triangular structures for numerical simulations with periodic boundary conditions. As illustrated in Fig. 6, the acceleration of the red particle j was influenced by six surrounding blue -checked particles k where k ranges from 1–6. The remaining particles filled the entire simulation area in the same manner as these seven particles. At equilibrium velocity, all particles traveled rightward. The positions of these particles are represented by the vector $\vec{x}_j(t) = (x_j(t), y_j(t))$ where x_j and y_j are the longitudinal and lateral positions of jth particle at time t, respectively. The distance between the particles k and j is r_{kj}. φ is the angle measured around the particle j. The direction vector from particles j to k is expressed as $\vec{n}_{kj}$. In summary, $\vec{x}_k - \vec{x}_j = r_{kj}\vec{n}_{kj}$.

Let a be the sensitivity parameter, constant value $\vec{V}_0$ the "desired velocity," and $\vec{F}$ the interaction between particles. The acceleration of particles following the 2D OVM is

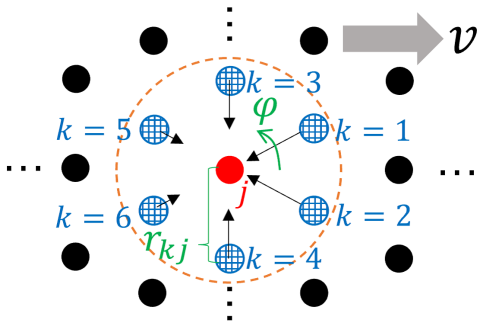

Figure 6 Configuration of Particles that 2D OVM considers.

formulated as follows:

$$\frac{d^2}{dt^2}\vec{x}_j = a\left[\left\{\vec{V}_0 + \sum_k \vec{F}(\vec{x}_k - \vec{x}_j)\right\} - \frac{d}{dt}\vec{x}_j\right] \tag{5}$$

where

$$\vec{F}(\vec{x}_k - \vec{x}_j) = f(r_{kj})(1+\cos\varphi)\vec{n}_{kj}, \tag{6}$$

$$f(r_{kj}) = \alpha[\tanh\beta(r_{kj} - b) + c] \tag{7}$$

where α, β, b, and c are constants. The vector $\vec{F}$ represents the varying component of the optimal velocity. As shown in Eq. 6, it depends on the direction φ and the distance r_{kj} of the particle. The constants α, β, b, and c are parameters of the function f, which describes the variation due to r_{kj}. The constants in Eq. 7 were set to the values used in the 2D OVM [33]: $\alpha = 0.25$, $\beta = 2.5$, $b = 1.0$, and $c = -1.0$. Consequently, $f\left(r_{kj}\right)$ always takes a negative value.

When the longitudinal wave originates from the direction $\varphi = 0$ in [33], the linear stability condition is expressed as

$$a > 2\{1+\cos(\theta s)\}\frac{(A_1 - A_5)^2}{A_1 + A_5} \tag{8}$$

where $A_k = \left.\frac{\partial F_x}{\partial(x_k - x_j)}\right|_{\text{eq}}$ and "eq" means the equilibrium state. θ represents the wavenumber.

In the following section, we describe the process for obtaining stability conditions for use in the stability analysis of the modified model. First, we assume an equilibrium flow, meaning thatEq. 5 is equal to zero. Note that

$$\overline{\vec{x}_j} = \vec{X}_j + \bar{\vec{v}}t \tag{9}$$

where $\vec{X}_j$ is a constant position

$$\vec{X}_j = \begin{pmatrix} X_j \\ Y_j \end{pmatrix}, \tag{10}$$

and

$$\vec{\bar{v}} = \begin{pmatrix} \overline{v_x} \\ \overline{v_y} \end{pmatrix} \tag{11}$$

is a constant-velocity vector under equilibrium flow. Variables with a bar above denote equilibrium variables. Let $\Delta x_j = (\Delta x_j, \Delta y_j)$ be a small fluctuation in the particle j. Then we obtain

$$\frac{d^2}{dt^2}\Delta x_j = a\sum_k \left\{A_k(\Delta x_k - \Delta x_j) + B_k(\Delta y_k - \Delta y_j) - \frac{d}{dt}\Delta x_j\right\}, \tag{12}$$

$$\frac{d^2}{dt^2}\Delta y_j = a\sum_k \left\{C_k(\Delta x_k - \Delta x_j) + D_k(\Delta y_k - \Delta y_j) - \frac{d}{dt}\Delta y_j\right\} \tag{13}$$

where $A_k = \frac{\partial F_x}{\partial(x_k - x_j)}\Big|_{\text{eq}}$, $B_k = \frac{\partial F_x}{\partial(y_k - y_j)}\Big|_{\text{eq}}$, $C_k = \frac{\partial F_y}{\partial(x_k - x_j)}\Big|_{\text{eq}}$, and $D_k = \frac{\partial F_y}{\partial(y_k - y_j)}\Big|_{\text{eq}}$.

Let

$$\Delta x_j = e^{i(\theta(X_j + pY_j) - \omega t)}, \tag{14}$$

$$\Delta y_j = p\Delta x_j \tag{15}$$

be the fluctuation in the longitudinal mode, where $i = \sqrt{-1}$ represents the imaginary unit and $\theta \in [-\pi, \pi]$ denotes the dimensionless wave number. The term $\omega = \alpha + i\beta$ consists of the angular frequency of the linear oscillation (negative value of α) and the oscillation growth parameter (β). The disturbance $e^{i(\theta(X_j + pY_j) - \omega t)}$ assumes that the region where the particles are located is periodic. This periodicity enables the determination of whether a small disturbance is amplified as it propagates between particles over an extended period. As p is defined by $\tan\varphi$ and denotes the direction of the longitudinal wave, $p = 0$. Then, we obtain the dispersion relation as

$$\omega^2 - ia\omega - 2aA_1\left(e^{i\theta S} - 1\right) - 2aA_5\left(e^{-i\theta S} - 1\right) = 0 \tag{16}$$

where $S = X_1 - X_j$ is the relative x position of particle 1 relative to j. In no-lane traffic, speed disturbances also occur in the lateral direction of the road. However, stability analysis was conducted in the $p = 0$ direction, as disturbances primarily occurring in the longitudinal direction of the road influence following vehicles, ultimately leading to congestion. The system is considered stable when the imaginary part of $\omega < 0$. This condition requires that

$$f_{\text{OVM}} = \frac{64}{a^2}(A_1 - A_5)^2(1 + \cos(\theta S)) - \frac{32}{a}(A_1 + A_5) < 0. \tag{17}$$

Eq. 17 can be rearranged to obtain a stability condition:

$$g_{\text{OVM}} = 2\{1 + \cos(\theta S)\}\frac{(A_1 - A_5)^2}{A_1 + A_5} - a < 0. \tag{18}$$

4.2. Modification of 2D OVM to Apply Varying Response Time

Fig. 7 depicts the variation in the sensitivity of the 2D OVM. As described in Sec. 1, response time can be regarded as part of the time duration required for velocity adjustment. In this study, we considered the adjustment duration as the sum of the time required for drivers to respond to the behavior of leading vehicles and the time needed to operate their pedals. The adjustment duration is denoted as T, which is the inverse of the sensitivity a in the 2D OVM, as shown in Fig. 7. The operation and response times are represented by T_{vadj} and τ, respectively. The varying sensitivity is denoted as a_{var}, and its inverse is the varying adjustment duration T_{var}. The variable a_{var} (the reciprocal of T_{var}) changes with the response time τ and represents the sensitivity of speed adjustment relative to the leader in the 2D OVMVS.

Here, we define T_{var} as the sum of the response time τ and the "constant" operation duration T_{vadj}. To determine the value of T_{vadj}, we subtracted the virtual response time $\tau_{0,0}$—which corresponds to τ when both dx and dy are zero—from the constant T in the 2D OVM. Notably, the constants T and a are varied in Sec. 5 to analyze the phase diagram.

The response time $\tau_{0,0}$ represents the response time in a hypothetical scenario where the following vehicle and the leading vehicle occupy the same space simultaneously. Although such a scenario does not occur in reality, $\tau_{0,0}$ is derived as an extrapolated result using the fitting function. We define T_{vadj} as the constant duration between the moment the driver perceives the leader's deceleration (after the response time τ) and the initiation of their operation. The reciprocal of the sensitivity a_{var} in 2D OVMVS, denoted as T_{var}, accounts for both T_{vadj} and the variable response time τ. That is, we assume $1/a_{\mathrm{var}} = T_{\mathrm{var}} = T_{\mathrm{vadj}} + \tau$. Since the response time τ is measurable in this study, it is necessary to determine T_{vadj}. Meanwhile, the reciprocal of the sensitivity a in the 2D OVM, denoted as T, is assumed to include the same T_{vadj} along with a constant response time. To determine T_{vadj}, it is essential to define the "constant response time" embedded in the sensitivity of the 2D OVM. Although it is unclear which specific values of dx and dy this "constant response time" corresponds to, we considered the scenario in which T_{vadj} is maximized, that is, when $(dx, dy) = (0, 0)$. By subtracting $\tau_{0,0}$, we examined the case where sensitivity is at its lowest when the variable τ is added. Furthermore, in the 2D OVMVS, τ is fitted as a function of dx and dy, with $(dx, dy) = (0, 0)$ as the origin. Subtracting $\tau_{0,0}$ also simplifies the analysis.

Although we varied the response time or sensitivity in the 2D OVM for each particle based on its relative position from particle j, the sensitivity in the original 2D OVM, denoted as a, remained constant and was independent of the summation in the formulation. As a result, the original 2D OVM is not formulated as

$$\frac{d^2}{dt^2}\vec{x}_j = \sum_k a\left[\left\{\vec{V}_0 + \vec{F}(\vec{x}_k - \vec{x}_j)\right\} - \frac{d}{dt}\vec{x}_j\right] \tag{19}$$

Therefore, we recapture the original 2D OVM as:

$$\frac{d^2}{dt^2}\vec{x}_j = \sum_{k=1}^{K} a\left[\left\{\frac{\vec{V}_0}{K} + \vec{F}(\vec{x}_k - \vec{x}_j)\right\} - \frac{1}{K}\frac{d}{dt}\vec{x}_j\right], \tag{20}$$

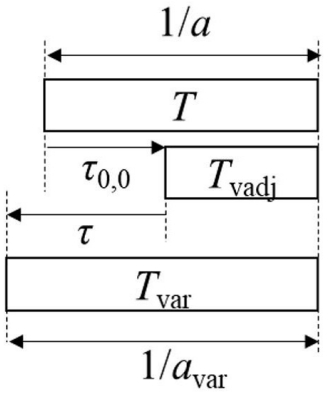

Figure 7 Time duration adjustment in the sensitivity variation method.

k is the index of a particle that influences particle j, and K is the maximum number of such particles. Based on this formulation, we obtain a 2D OVM by varying the sensitivity as

$$\frac{d^2}{dt^2}\vec{x}_j = \sum_{k=1}^{K} a_k \left[\left\{ \frac{\vec{V}_0}{K} + \vec{F}(\vec{x}_k - \vec{x}_j) \right\} - \frac{1}{K}\frac{d}{dt}\vec{x}_j \right]. \tag{21}$$

Hereinafter, this model is referred to as the 2D OVM with varying sensitivities (2D OVMVS). Assuming the same scenario as in [33], where a particle is surrounded by six others (i.e., $K = 6$ and k is from 1 to 6), Eq. 21 transforms into

$$\frac{d^2}{dt^2}\vec{x}_j = \sum_{k=1}^{6} a_k \left[\left\{ \frac{\vec{V}_0}{6} + \vec{F}(\vec{x}_k - \vec{x}_j) \right\} - \frac{1}{6}\frac{d}{dt}\vec{x}_j \right]. \tag{22}$$

As previously mentioned, the primary objective of this study is to determine the influence of response time on the stability of the assumed 2D traffic by comparing the stability outcomes obtained from the 2D OVM and 2D OVMVS. Hence, the subsequent analysis is based on the 2D OVM with six particles, for which stability conditions have already been established.

4.3. Derivation of Stability Condition

Here, we introduce an approximate procedure to obtain a stability condition for 2D OVMVS. All the procedure is described in App. A. In Sec. 4.1, we assumed the small fluctuation of j under the equilibrium state. The same procedure, ignoring second-order microquantities, induces

$$\begin{aligned} \frac{d^2}{dt^2}\Delta x_j = \sum_k \Bigg[& a_{ke}\{A_k(\Delta x_k - \Delta x_j) \\ & + B_k(\Delta y_k - \Delta y_j) - \frac{1}{6}\frac{d}{dt}\Delta x_j\} \\ & + \left\{ \xi_{ke}(\Delta x_k - \Delta x_j) + \eta_{ke}(\Delta y_k - \Delta y_j) \right\} \left(-\frac{1}{6}\frac{d}{dt}\Delta x_j \right) \Bigg], \end{aligned} \tag{23}$$

and

$$\begin{aligned}\frac{d^2}{dt^2}\Delta y_j = \sum_k \Bigg[a_{ke}\{C_k(\Delta x_k - \Delta x_j) \\ + D_k(\Delta y_k - \Delta y_j) - \frac{1}{6}\frac{d}{dt}\Delta y_j\} \\ + \left\{\xi_{ke}(\Delta x_k - \Delta x_j) + \eta_{ke}(\Delta y_k - \Delta y_j)\right\}\left(-\frac{1}{6}\frac{d}{dt}\Delta y_j\right)\Bigg],\end{aligned} \tag{24}$$

where $a_{ke} = a(\vec{X}_k - \vec{X}_j)$, $\xi_{ke} = \frac{\partial a_k}{\partial(x_k - x_j)}\Big|_{\text{eq}}$, and $\eta_{ke} = \frac{\partial a_k}{\partial(y_k - y_j)}\Big|_{\text{eq}}$. The terms ξ_{ke} and η_{ke} multiplied by $-\frac{1}{6}\frac{d}{dt}\Delta x_j$ or $-\frac{1}{6}\frac{d}{dt}\Delta y_j$ can be ignored because they are second-order microquantities.

By introducing a small fluctuation in particle j to Eq. 14 and Eq. 15, we obtain the dispersion relation

$$\omega^2 + 2a_{1e}\left\{A_1(e^{i\theta S} - 1) + \frac{i\omega}{6}\right\} + 2a_{5e}\left\{A_5(e^{i\theta S} - 1) + \frac{i\omega}{6}\right\} + 2a_{3e}\frac{i\omega}{6} = 0. \tag{25}$$

Similarly, by obtaining Eq. 17, we obtain the condition wherein the imaginary part of ω is less than zero.

$$\begin{aligned}f_{\text{OVMVS}} = \left\{\frac{72}{(a_{1e} + a_{3e} + a_{5e})^2}\right\}^2 (A_1 a_{1e} - A_5 a_{5e})^2 (1 + \cos(\theta S)) \\ - \frac{288}{(a_{1e} + a_{3e} + a_{5e})^2}(A_1 a_{1e} + A_5 a_{5e}) < 0.\end{aligned} \tag{26}$$

Note that Eq. 17 and Eq. 26 can be directly compared, as no constants or variables were altered under the condition that the imaginary part of $\omega < 0$. Rearranging Eq. 26, we obtain the stability condition

$$g_{\text{OVMVS}} = \{1 + \cos(\theta S)\}\frac{(A_1 a_{1e} - A_5 a_{5e})^2}{A_1 a_{1e} + A_5 a_{5e}} - \frac{(a_{1e} + a_{3e} + a_{5e})^2}{18} < 0. \tag{27}$$

5. Effect of Varying Response Time on Stability

5.1. Stability Shift due to the Varying Response Time

Fig. 8(a) and Fig. 8(b) illustrate the stable and unstable regions for parameter sets of sensitivity and distance. In Fig. 8(a), the values of g_{OVM} in Eq. 18 are shown. As evident, under relatively low sensitivity within a certain range (i.e., a prolonged duration for velocity adjustment), the flow became unstable within a specific range of distances between particles.

Fig. 8(b) presents the values of g_{OVMVS} from Eq. 27. The vertical axis represents the "standard a for a_{var}", which denotes the value of a used to compute a_{var} as illustrated

in Fig. 7. In other words, a_{var} in 2D OVMVS is computed by subtracting $\tau_{0,0}$ from the reciprocal of this "standard a" and then adding τ. Additionally, a constant a was applied to particles behind the focusing particle ($k = 5$ and 6) as only the response time variations of "leaders positioned ahead of the ego vehicle were observed. In Fig. 8(b), the value of a for particles $k = 5$ and 6 (a_{behind}) was equal to the standard a. No significant difference was observed between the plots of g_{OVM} and g_{OVMVS} in Fig. 8(a) and Fig. 8(b), respectively.

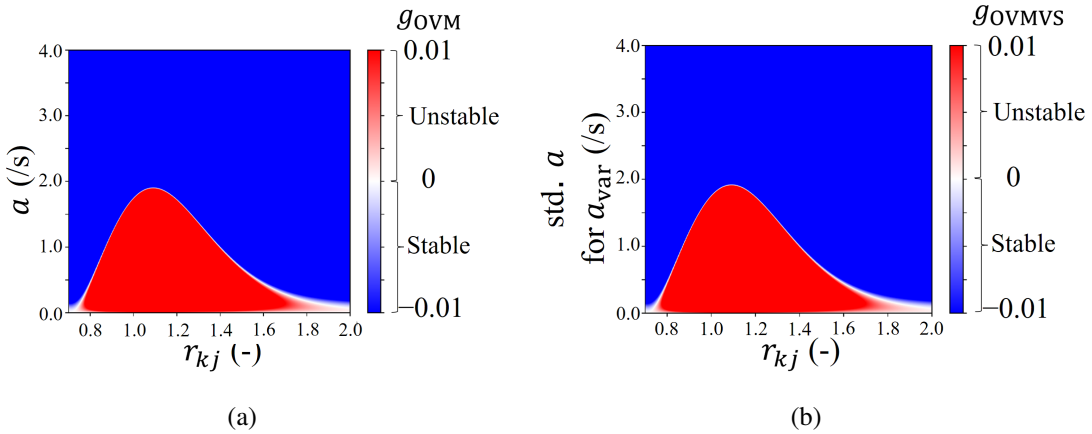

Figure 8 Phase diagrams for (a) 2D OVM and (b) 2D OVMVS.

As described in Sec. 4.3, Eq. 17 and Eq. 26 can be directly compared. Therefore, we plotted the comparison results in Fig. 9, which is divided into four regions based on the stability definitions outlined in Tab. 4 for both OVM and OVMVS. Here, the term "shift" in Tab. 4 indicates whether the values of f_{OVMVS} increased or decreased relative to f_{OVM}, that is, whether the introduction of a varying response time led to stabilization or destabilization of the flow. However, stating that the flow is stabilized does not necessarily imply that the system is stable overall. The term "stabilize" in Tab. 4 means that the stability index f_{OVM} of the 2D OVM is greater than the stability index f_{OVMVS} of the 2D OVMVS. If either f_{OVM} or f_{OVMVS} is less than zero, the flow can be considered stable, and smaller values of f_{OVM} or f_{OVMVS} indicate a faster convergence of velocity disturbances. Even when the values are greater than zero, smaller values of f_{OVM} or f_{OVMVS} that are closer to zero suggest a slower growth rate of disturbances. Conversely, the term "destabilize" represents the opposite situation.

In Tab. 4, the term "more stable" means that the region was already stable in the 2D OVM but becomes even more stable in the 2D OVMVS when response time variation is considered, as indicated by a smaller f_{OVMVS}. "More unstable" means that the region was already unstable in the 2D OVM but becomes even more unstable in the 2D OVMVS. "Still stable" means that the region was stable in the 2D OVM, though it remains stable even if it is destabilized in the 2D OVMVS. "Still unstable" means that the region was unstable in the 2D OVM, though it remains unstable even if it is stabilized in the 2D OVMVS. The regions in Table 3 are defined based on the above criteria. Note that Areas V and VI appear in Sec. 5.2 afterward.

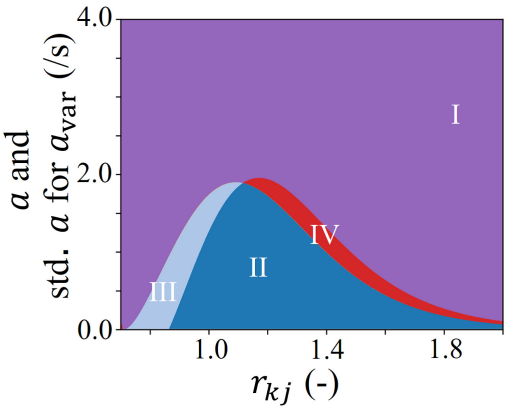

Figure 9 Trend variation when applied the varying response time.

Table 4 Phase diagram shift due to the varying response time

Area	Stability in OVM	shift	Stability in OVMVS
I	Stable	Stabilize	More stable
II	Unstable	Destabilized	More unstable
III	Unstable	Stabilized	Still unstable
IV	Stable	Destabilized	Still stable
V	Stable	Destabilized	Change to unstable
VI	Unstable	Stabilized	Change to stable

From Fig. 9 and Tab. 4, we conclude that the introduction of a varying response time did not alter the overall stability mapping. However, in most phase diagrams, the stable region became more stable (Area I), while the unstable region became more unstable (Area II). This suggests that incorporating response time variability accelerated the transition between flow states when small disturbances occurred.

5.2. Sensitivity Analysis on Stability Shift

In Sec. 5.1, we assumed that a_{behind} was equal to the standard a, and that $r_{kj} = 1$ corresponded to 1 m in the response time distribution shown in Fig. 5.

However, a_{behind} would be smaller than the standard a because drivers typically react more slowly to vehicles behind them compared to those in front. Thus, we formulated the relationship between the standard a and a_{behind} as

$$a_{\text{behind}} = \frac{\text{standard } a}{k_{\text{behind}}} \tag{28}$$

where k_{behind} is a coefficient. We conducted a sensitivity analysis. when $k_{\text{behind}} = 1$ and 1.3.

The distance r_{kj} used in 2D OVM and OVMVS is inherently dimensionless, while the distances defined on the DS are measured in meters. To bridge this gap, we introduced a

proportionality coefficient k_{dist}, where the dimensionless length in 2D OVM and OVMVS is denoted as R, and the corresponding length on the DS, measured in meters, is denoted as D. Additionally, the headways between vehicles were not smaller than 1 m, for example, in the free-flow phase. Based on this, we formulated the relationship between the distance $D\,(\mathrm{m})$ in the response time distribution shown in Fig. 5 (where response time depends on the leader location), and the dimensionless distance $R\,(-)$ in Fig. 6 as

$$D\,(\mathrm{m}) = R\,(-) \times k_{\text{dist}}\,(\mathrm{m}), \tag{29}$$

where $k_{\text{dist}}\,(\mathrm{m})$ is a coefficient greater than 1 m. Since Fig. 5 was obtained from DS, wherein distances are specified in meters, we have added the (m) unit to D.

We conducted a sensitivity analysis for $k_{\text{dist}} = 0.7\,\mathrm{m}$, 1 m, 2 m and 3 m. Fig. 10 shows the shift in the phase diagram owing to the varying response time for respective k_{behind} and k_{dist}. Areas I–V indicate the shifts in the phase diagram, as shown in Tab. 4. First, the increase in k_{behind} affected the shift. The respective subfigures for $k_{\text{behind}} = 1.3$ exhibited larger area IV than those for $k_{\text{behind}} = 1.0$. Although the stability was disturbed in Area IV, it was still stable. Furthermore, the figures for $k_{\text{behind}} = 1.3$ exhibited an area V, where the stability changed to unstable.

Moreover, an increase in k_{dist} exerted a similar effect on $k_{\text{behind}} = 1$. In other words, both areas IV and V increased. Besides, $k_{\text{dist}} < 1$ also corresponds to drivers who have a quicker response time than the subjects because they are more used to traffic with weak-lane discipline. In both cases of $k_{\text{behind}} = 1.0$ and 1.3, the trends in the phase diagrams remained unchanged.

In summary, in the 2D OVMVS model, the equilibrium hexagonal arrangement collapsed more quickly in areas classified as unstable in the 2D OVM model. Furthermore, the unstable region expanded within a certain range of headway distances in the 2D OVMVS compared to the 2D OVM.

6. Discussion

In high -density conditions where overtaking is impossible, the deceleration wave is amplified and propagates through the unstable region. However, instability does not necessarily indicate the formation of stop-and-go waves; rather, it signifies that disturbances are amplified, leading to the breakdown of the hexagonal configuration.

In scenarios where overtaking is possible, the findings of this study suggest that actual 2D traffic is less likely to maintain a steady formation compared to previous models that do not account for variations in response time. In other words, 2D traffic exhibits a greater tendency toward overtaking due to the distribution of response times, even in the absence of motorcycles or autorickshaws that can easily maneuver through traffic.

Previous studies have explored the factors influencing response time. For instance, [42] interrevealed that response time varies depending on road geometry. Additionally, studies examining the impact of response time on the stability of vehicle platoons include [43], which used nonlinear analysis of the OVM to show that a decrease in sensitivity (the inverse of response time, as used in this study) expands the unstable region. Kesting et

al. [44] introduced numerical update intervals in addition to response time, demonstrating that an increase in either factor leads to instability in vehicle platoons. Furthermore, they found that both factors influence stability in a similar manner. Similarly, [45] assumed that driver response time varies due to temporal and spatial anticipation, which enhances stability. Their simulation-based stability analysis identified response time thresholds beyond which speed disturbances result in collisions.

A study strongly related to the present work is that of Tomoeda et al. [46], which, based on real-world data, suggested that response time decreases as traffic density increases. Tomoeda et al. [46] focused on lane-based highway traffic, and their findings align with the longitudinal observations of the present study. Moreover, incorporating this response time variation into the Payne model led to the conclusion that traffic flow stability becomes density-dependent, where disturbances that grow at low density are stabilized at high density. Although the study by Tomoeda et al. focused on lane-based traffic, its conclusions correspond to Area II and the region of small r_{kj} within Area I in Figure 9 of this paper.

The findings of this study are consistent with prior research on the effects of response time on traffic flow stability, particularly regarding trends in longitudinal headway and response time variation. However, unlike previous studies, the present work considers no-lane-based traffic. In no-lane-based traffic, it is hypothesized that speed disturbances arising from instability may not only lead to stop-and-go waves or collisions but also trigger overtaking and passing behavior. The novel contributions of this study include (1) demonstrating that response time varies not only with longitudinal headway but also with lateral headway, (2) fitting these variations into functions implemented as part of the 2D OVMVS, and (3) showing through stability analysis that the distribution of response time induces the early collapse of hexagonal configurations and promotes the occurrence of overtaking and passing.

Regarding future research, further investigation is needed to determine how the inability to maintain formation affects congestion in 2D traffic. To the best of our knowledge, there are currently no established indicators for assessing whether disturbances are amplified or mitigated by the active alternation of vehicle order that occurs in traffic at densities where overtaking is possible.

Additionally, this study did not measure the distribution of reaction time to the vehicle behind the ego vehicle; instead, it assumed it to be constant. Although the sensitivity analysis provided an approximate trend, the distribution of reaction time to the vehicle behind the ego vehicle should be measured and incorporated into the sensitivity parameter a_{var}.

7. Conclusion

To enhance the replication and comprehension of traffic scenarios characterized by weak lane discipline, this study investigated the variability in response time to both longitudinal and lateral shifts concerning the relative position of the leader. Through experimentation utilizing a DS, we demonstrated that response time is influenced by the relative position

of the leader. Additionally, we applied functional fitting techniques to model the response time distribution, identifying that linear and exponential functions were suitable for the longitudinal and lateral directions, respectively.

Moreover, we expanded the formulation of the 2D OVM and introduced the concept of 2D OVMVS, which incorporates variable sensitivity corresponding to the variable response time. We subsequently derived the stability condition for the 2D OVMVS.

A comparative analysis of the phase diagrams obtained with the 2D OVM and 2D OVMVS, along with a sensitivity analysis of stability shift, revealed that the 2D OVMVS exhibited a wider unstable region in the phase diagram and lower stability, even within stable regions than the 2D OVM. This finding suggests that in 2D traffic characterized by weak lane discipline, vehicle equilibrium is more vulnerable to disruption. The distribution of response times appears to undermine stability, even within the framework of linear analysis. This highlights the contribution of response time variability to the tendency of vehicles in 2D traffic to engage in frequent overtaking or weaving maneuvers, particularly as density increases beyond the aligned free-flow phase.

This study demonstrates that the distribution of response times negatively affects the stability of 2D traffic. To counteract this destabilizing effect [47], potential strategies include enhancing drivers' awareness of their vehicle's historical speed differentials relative to desired speeds, utilizing auditory alerts (e.g., honks) from following vehicles, and implementing driver assistance systems capable of monitoring distances between multiple vehicles ahead [48].

However, further investigation is required to assess the impact of this inability to maintain formation on congestion occurrence within 2D traffic. In this context, nonlinear analysis is a crucial avenue for future research. Additionally, the development of new evaluation metrics is imperative to determine whether disturbances are amplified or mitigated in traffic scenarios characterized by dynamic variations in vehicle formation.

Regarding the stability discussion using 2D OVM and OVMVS, this study examined whether velocity perturbations from the equilibrium state grow or dissipate. As a result, we successfully found that the initiation of overtaking and passing maneuvers from a steady 2D traffic state is accelerated by the distribution of response times. However, in heterogeneous 2D traffic, such as those observed in developing countries, it remains unclear how response time variability and differences among individual vehicles influence overall system behavior. Furthermore, this study does not address the impact of response time distribution on macroscopic traffic characteristics (such as density vs. flow) in non-equilibrium states where overtaking, passing, and velocity perturbations already exist.

To investigate the effect of response time distribution on stability, hexagonal vehicle arrangements were applied in this study to facilitate comparison with the 2D OVM, for which a theoretical measure of stability has already been established. Additionally, the 2D OVM and 2D OVMVS can maintain steady states through hexagonal configurations. Developing a model capable of preserving formations in other heterogeneous vehicle arrangements would further clarify the influence of response times on more realistic 2D traffic scenarios. The microscopic model for lane-less traffic [34] discusses stability under time-varying leader-follower relationships and configurations beyond the hexagonal arrangement. If this model could integrate variations in response time, it would enable a

more realistic theoretical evaluation of the stability of no-lane traffic.

Moreover, several improvements should be implemented in future DS experiments. First, measuring response times while accounting for velocity differences between the leader and follower is essential for further understanding traffic stability in environments lacking lane discipline. Second, this study assumed symmetrical response time distributions for the left and right sides; future research should validate this assumption. Third, in this experiment, response time was measured based on a single leader. Consequently, there may be deviations from actual response times in situations where multiple vehicles influence driver behavior, as is commonly observed in real-world traffic or 2D OVM simulations. Conducting further experiments with participants is necessary to refine the model.

Acknowledgements This work was supported by JSPS KAKENHI Grant Numbers 18H05923 (A. N.), 19K15246 (A. N.), 23K13512 (A. N.), and 23K11139 (A. Y.), and the Suzuki Foundation (A. N.).

Ethics Statement The Ritsumeikan University Ethics Review Committee for Medical and Health Research Involving Humans approved the experiment using a driving simulator in this study. All participants gave written informed consent to participate in the study.

Author Contributions Akihito Nagahama: Conceptualization, Methodology, Software, Formal analysis, Investigation, Data curation, Writing – Original draft, Visualization, Funding acquisition / Akiyasu Tomoeda: Validation, Formal analysis, Writing – review and editing, Funding acquisition / Takahiro Wada: Validation, Resources, Writing – review and editing.

References

[1] Elmansouri, O., Almhroog, A., Badi, I.: Urban transportation in libya: An overview. Transportation research interdisciplinary perspectives **8**, 100161 (2020)

[2] Samal, S.R., Mohanty, M., Santhakumar, S.M.: Adverse effect of congestion on economy, health and environment under mixed traffic scenario. Transportation in Developing Economies **7**(2), 15 (2021)

[3] Fattah, M.A., Morshed, S.R., Kafy, A.A.: Insights into the socio-economic impacts of traffic congestion in the port and industrial areas of chittagong city, bangladesh. Transportation Engineering **9**, 100122 (2022)

[4] Farooq, M., Ramzan, M., Zakir, R.: Barriers in enforcement of traffic regulations and risk-taking behaviour: A study of public service vehicle drivers. Pakistan Social Sciences Review **5**(1), 858–869 (2021)

[5] Susanty, A., Purwanggono, B., Putri, V.A.: The barriers to the implementation of intelligent transportation system at semarang city. Procedia Computer Science **191**, 312–319 (2021)

[6] Tomaszewska, E.J.: Barriers related to the implementation of intelligent transport systems in cities-the polish local government's perspective. Engineering Management in Production and Services **13**(4), 131–147 (2021)

[7] Shaaban, K., Elamin, M., Alsoub, M.: Intelligent transportation systems in a developing country: benefits and challenges of implementation. Transportation Research Procedia **55**, 1373–1380 (2021)

[8] Nguyen, P.T., Nguyen, T.A., Tran, T.H.T.: Barrier factors affecting development of intelligent transport system projects. Journal of process management and new technologies **9**(3-4), 100–120 (2021)

[9] Singh, G., Bansal, D., Sofat, S.: Intelligent transportation system for developing countries-a survey. International Journal of Computer Applications **85**(3), 34–38 (2014)

[10] Behruz, H., Chavoshy, A., Mozaffari, G., et al.: Challenges of implementation of intelligent transportation systems in developing countries: case study–tehran. WIT Transactions on Ecology and the Environment **179**, 977–987 (2013)

[11] Munigety, C.R., Gupta, P.A., Gurumurthy, K.M., Peeta, S., Mathew, T.V.: Vehicle-type dependent car following model using spring-mass-damper dynamics for heterogeneous traffic. In: Transportation Research Board 95th Annual Meeting, 16-5025 (2016)

[12] Ossen, S., Hoogendoorn, S.P.: Heterogeneity in car-following behavior: Theory and empirics. Transportation research part C: emerging technologies **19**(2), 182–195 (2011)

[13] Sayer, J.R., Mefford, M.L., Huang, R.W.: The Effects of Lead-Vehicle Size on Driver Following Behavior: Is Ignorance Truly Bliss? In: Proceedings of the Second InternationalDriving Symposyum on Human Factors in Driver Assesment, Training and Vehicle Design, pp. 221–225 (2003)

[14] Sarvi, M.: Heavy commercial vehicles-following behavior and interactions with different vehicle classes. Journal of advanced transportation **47**(6), 572–580 (2013)

[15] Aghabayk, K., Young, W., Sarvi, M., Wang, Y.: Examining vehicle interactions during a vehicle-following manoeuvre. In: Australasian Transport Research Forum (ATRF), 34th, 2011, Adelaide, South Australia, Australia, vol. 34 (2011)

[16] Nagahama, A., Yanagisawa, D., Nishinari, K.: Dependence of driving characteristics upon follower–leader combination. Physica A: Statistical Mechanics and its Applications **483**, 503–516 (2017)

[17] Mason, A.D., Woods, A.W.: Car-following model of multispecies systems of road traffic. Physical Review E **55**(3), 2203 (1997)

[18] Yang, D., Jin, J., Ran, B., Pu, Y., Yang, F.: Modeling and analysis of car-truck heterogeneous traffic flow based on intelligent driver car-following model. In: Transportation Research Board 92nd Annual Meeting, 13-2358 (2013)

[19] Ngoduy, D.: Effect of the car-following combinations on the instability of heterogeneous traffic flow. Transportmetrica B: transport dynamics **3**(1), 44–58 (2015)

[20] Chen, D., Ahn, S., Bang, S., Noyce, D.: Car-Following and Lane-Changing Behavior Involving Heavy Vehicles. Transportation Research Record: Journal of the Transportation Research Board (2561), 89–97 (2016)

[21] Nagatani, T.: Modified kdv equation for jamming transition in the continuum models of traffic. Physica A: Statistical Mechanics and Its Applications **261**(3-4), 599–607 (1998)

[22] Mohan, R., Ramadurai, G.: Heterogeneous traffic flow modelling using second-order macroscopic continuum model. Physics Letters A **381**(3), 115–123 (2017)

[23] Chattopadhyay, S.N., Gupta, A.K.: Anticipating tipping points for disordered traffic: Critical slowing down on the onset of congestion. arXiv preprint arXiv:2401.09364 (2024)

[24] Ahmed, K., Ben-Akiva, M., Koutsopoulos, H., Mishalani, R.: Models of freeway lane changing and gap acceptance behavior. Transportation and traffic theory **13**, 501–515 (1996)

[25] Kesting, A., Treiber, M., Helbing, D.: General lane-changing model MOBIL for car-following models. Transportation Research Record **1999**(1), 86–94 (2007)

[26] Schönauer, R., Stubenschrott, M., Huang, W., Rudloff, C., Fellendorf, M.: Modeling concepts for mixed traffic: Steps toward a microscopic simulation tool for shared space zones. Transportation research record **2316**(1), 114–121 (2012)

[27] Tang, J., Liu, F., Zhang, W., Ke, R., Zou, Y.: Lane-changes prediction based on adaptive fuzzy neural network. Expert Systems with Applications **91**, 452–463 (2018)

[28] Oketch, T.: New modeling approach for mixed-traffic streams with nonmotorized vehicles. Transportation Research Record: Journal of the Transportation Research Board (1705), 61–69 (2000)

[29] Kanagaraj, V., Treiber, M.: Self-driven particle model for mixed traffic and other disordered flows. Physica A: Statistical Mechanics and its Applications **509**, 1–11 (2018)

[30] Jiang, N., Yu, B., Cao, F., Dang, P., Cui, S.: An extended visual angle car-following model considering the vehicle types in the adjacent lane. Physica A: Statistical Mechanics and its Applications **566**, 125665 (2021)

[31] Yu, B., Zhou, H., Wang, L., Wang, Z., Cui, S.: An extended two-lane car-following model considering the influence of heterogeneous speed information on drivers with different characteristics under honk environment. Physica A: Statistical Mechanics and its Applications **578**, 126022 (2021)

[32] Xue, Y., Wang, L., Yu, B., Cui, S.: A two-lane car-following model for connected vehicles under connected traffic environment. IEEE Transactions on Intelligent Transportation Systems (2024)

[33] Nakayama, A., Hasebe, K., Sugiyama, Y.: Instability of pedestrian flow and phase structure in a two-dimensional optimal velocity model. Physical Review E **71**(3), 036121 (2005)

[34] Mulla, A.K., Joshi, A., Chavan, R., Chakraborty, D., Manjunath, D.: A microscopic model for lane-less traffic. IEEE Transactions on Control of Network Systems **6**(1), 415–428 (2018)

[35] Eriksen, C.W., St. James, J.D.: Visual attention within and around the field of focal attention: A zoom lens model. Perception & psychophysics **40**(4), 225–240 (1986)

[36] Stoffer, T.H.: Attentional focussing and spatial stimulus-response compatibility. Psychological research **53**(2), 127–135 (1991)

[37] Nagahama, A., Wada, T.: Response time and deceleration affected by lateral shift of leaders in vehicular traffic with weak lane discipline. In: Traffic and Granular Flow 2019, pp. 539–546. Springer (2020)

[38] Treiber, M., Kesting, A.: Traffic Flow Dynamics. Springer (2013)

[39] Authority, R.S.: The two-second rule (2007). URL https://web.archive.org/web/20120309213451/http://www.rotr.ie/rules-for-driving/speed-limits/speed-limits_2-second-rule.html. Last visited: November 11, 2024

[40] Sayer, J., LeBlanc, D., Bogard, S., Funkhouser, D., Bao, S., Buonarosa, M.L., Blankespoor, A., et al.: Integrated vehicle-based safety systems field operational test: Final program report. Tech. rep., United States. Joint Program Office for Intelligent Transportation Systems (2011)

[41] Plewan, T., Rinkenauer, G.: Simple reaction time and size–distance integration in virtual 3d space. Psychological Research **81**, 653–663 (2017)

[42] Tawfeek, M.H.: Inter-and intra-driver reaction time heterogeneity in car-following situations. Sustainability **16**(14), 6182 (2024)

[43] Mousavi, S.S., Bahrami, S., Kouvelas, A.: Stability analysis for a platoon of vehicles with reaction-time delay. In: 2023 62nd IEEE Conference on Decision and Control (CDC), pp. 7767–7772. IEEE (2023)

[44] Kesting, A., Treiber, M.: How reaction time, update time, and adaptation time influence the stability of traffic flow. Computer-Aided Civil and Infrastructure Engineering **23**(2), 125–137 (2008)

[45] Kesting, A., Treiber, M.: Influence of reaction times and anticipation on the stability of vehicular traffic flow. IFAC Proceedings Volumes **39**(10), 205–210 (2006). doi:https://doi.org/10.3182/20060710-3-IT-4901.00034. URL https://www.sciencedirect.com/science/article/pii/S1474667016352168. 6th IFAC Workshop on Time Delay Systems

[46] Tomoeda, A., Shamoto, D., Nishi, R., Ohtsuka, K., Nishinari, K.: A new compressible fluid model for traffic flow with density-dependent reaction time of drivers. JSIAM Letters **1**, 72–75 (2009)

[47] Cui, S., Cao, F., Yu, B., Yao, B.: Modeling heterogeneous traffic mixing regular, connected, and connected-autonomous vehicles under connected environment. IEEE Transactions on Intelligent Transportation Systems **23**(7), 8579–8594 (2021)

[48] Nagatani, T.: Stabilization and enhancement of traffic flow by the next-nearest-neighbor interaction. Physical Review E **60**(6), 6395 (1999)

A. Stability condition of 2D OVMVS

The extended 2D OVM (2D OVMVS) is formulated as follows:

$$\frac{d^2}{dt^2}\vec{x}_j = \sum_k a_k \left[\left\{ \frac{\vec{V}_0}{6} + \vec{F}(\vec{x}_k - \vec{x}_j) \right\} - \frac{1}{6}\frac{d}{dt}\vec{x}_j \right]. \tag{30}$$

Herein, $a_k = a(\vec{x}_k - \vec{x}_j)$, which is a function of the relative position.

Let us assume Eq. 30 has a solution $\overline{\vec{x}_j}$ for the equilibrium flow under a hexagonal formation, where

$$\overline{\vec{x}_j} = \vec{X}_j + \overline{\vec{v}}t, \quad (\vec{X}_j\text{: constant vector}, \quad \overline{\vec{v}} = \begin{pmatrix} \overline{v_x} \\ \overline{v_y} \end{pmatrix}\text{: constant vector}).$$

Then, the solution satisfies

$$\vec{0} = \sum_k a_{ke} \left[\left\{ \frac{\vec{V}_0}{6} + \vec{F}(\vec{X}_k - \vec{X}_j) \right\} - \frac{1}{6}\overline{\vec{v}} \right],$$

i.e.,

$$0 = \sum_k a_{ke} \left[\left\{ \frac{V_0}{6} + F_x(\vec{X}_k - \vec{X}_j) \right\} - \frac{1}{6}\overline{v_x} \right] \tag{31}$$

$$0 = \sum_k a_{ke} \left[\left\{ F_y(\vec{X}_k - \vec{X}_j) \right\} - \frac{1}{6}\overline{v_y} \right], \tag{32}$$

where

$$a_{ke} = a(\vec{X}_k - \vec{X}_j)$$

Hereafter, they are referred to as $F_x(\vec{X}_k - \vec{X}_j) = F_{xe}$, $F_y(\vec{X}_k - \vec{X}_j) = F_{ye}$.

Substituting a small disturbance,

$$\vec{x}_j = \overline{\vec{x}_j} + \Delta\vec{x}_j, \quad \Delta\vec{x}_j = \begin{pmatrix} \Delta x_j \\ \Delta y_j \end{pmatrix}$$

into Eq. 30, we obtain

$$\frac{d^2}{dt^2}\vec{x}_j = \sum_k a_k\left((\overline{\vec{x}_k} - \overline{\vec{x}_j}) + (\Delta\vec{x}_k - \Delta\vec{x}_j)\right)\left[\frac{\vec{v}_0}{6} + \vec{F}\left((\overline{\vec{x}_k} - \overline{\vec{x}_j}) + (\Delta\vec{x}_k - \Delta\vec{x}_j)\right) - \frac{1}{6}\left(\frac{d}{dt}\Delta\vec{x}_j + \overline{\vec{v}}\right)\right]$$

$$\Leftrightarrow \frac{d^2}{dt^2}\Delta\vec{x}_j$$

$$= \sum_k \left[a_k\left((\vec{X}_k - \vec{X}_j) + (\Delta\vec{x}_k - \Delta\vec{x}_j)\right)\left\{\frac{\vec{V}_0}{6} + \vec{F}\left((\vec{X}_k - \vec{X}_j) + (\Delta\vec{x}_k - \Delta\vec{x}_j)\right) - \frac{1}{6}\left(\frac{d}{dt}\Delta\vec{x}_j + \overline{\vec{v}}\right)\right\}\right] \tag{33}$$

The first section using the wavy line in Eq. 33 can be expanded as

$$a_k(\vec{X}_k - \vec{X}_j) + \left.\frac{\partial a_k}{\partial(x_k - x_j)}\right|_{\vec{X}_k - \vec{X}_j}(\Delta x_k - \Delta x_j) + \left.\frac{\partial a_k}{\partial(y_k - y_j)}\right|_{\vec{X}_k - \vec{X}_j}(\Delta y_k - \Delta y_j)$$

$$= a_{ke} + \xi_{ke}(\Delta x_k - \Delta x_j) + \eta_{ke}(\Delta y_k - \Delta y_j).$$

Here we defined $a_k(\vec{X}_k - \vec{X}_j) = a_{ke}$, $\left.\frac{\partial a_k}{\partial(x_k - x_j)}\right|_{\vec{X}_k - \vec{X}_j} = \xi_{ke}$, and $\left.\frac{\partial a_k}{\partial(y_k - y_j)}\right|_{\vec{X}_k - \vec{X}_j} = \eta_{ke}$. The second section with wavy line in Eq. 33 can be expanded as

$$F_{xe} + \left.\frac{\partial F_x}{\partial(x_k - x_j)}\right|_{\vec{X}_k - \vec{X}_j}(\Delta x_k - \Delta x_j) + \left.\frac{\partial F_x}{\partial(y_k - y_j)}\right|_{\vec{X}_k - \vec{X}_j}(\Delta y_k - \Delta y_j),$$

and

$$F_{ye} + \left.\frac{\partial F_y}{\partial(x_k - x_j)}\right|_{\vec{X}_k - \vec{X}_j}(\Delta x_k - \Delta x_j) + \left.\frac{\partial F_y}{\partial(y_k - y_j)}\right|_{\vec{X}_k - \vec{X}_j}(\Delta y_k - \Delta y_j).$$

Substituting these values into Eq. 33,

$$\frac{d^2}{dt^2}\Delta x_j = \sum_k \left[\left\{a_{ke} + \xi_{ke}(\Delta x_k - \Delta x_j) + \eta_{ke}(\Delta y_k - \Delta y_j)\right\}\right.$$
$$\left.\left\{\frac{V_0}{6} + F_{xe} + A_k(\Delta x_k - \Delta x_j) + B_k(\Delta y_k - \Delta y_j) - \frac{1}{6}\left(\frac{d}{dt}\Delta x_j + \overline{v_x}\right)\right\}\right], \tag{34}$$

and

$$\frac{d^2}{dt^2}\Delta y_j = \sum_k \Bigg[\Big\{ a_{ke} + \xi_{ke}(\Delta x_k - \Delta x_j) + \eta_{ke}(\Delta y_k - \Delta y_j) \Big\} \Big\{ F_{ye} + C_k(\Delta x_k - \Delta x_j) + D_k(\Delta y_k - \Delta y_j) - \frac{1}{6}\Big(\frac{d}{dt}\Delta y_j + \overline{v_y}\Big) \Big\} \Bigg], \quad (35)$$

where $A_k = \frac{\partial F_x}{\partial(x_k - x_j)}\Big|_{\vec{X}_k - \vec{X}_j}$, $B_k = \frac{\partial F_x}{\partial(y_k - y_j)}\Big|_{\vec{X}_k - \vec{X}_j}$, $C_k = \frac{\partial F_y}{\partial(x_k - x_j)}\Big|_{\vec{X}_k - \vec{X}_j}$, and $D_k = \frac{\partial F_y}{\partial(y_k - y_j)}\Big|_{\vec{X}_k - \vec{X}_j}$.

Utilizing Eq. 31, and an approximation that ignores the second-order miniscule quantities, Eq. 34 can be transformed as follows:

$$\frac{d^2}{dt^2}\Delta x_j = \sum_k \Bigg[a_{ke} \Big\{ A_k(\Delta x_k - \Delta x_j) + B_k(\Delta y_k - \Delta y_j) - \frac{1}{6}\frac{d}{dt}\Delta x_j \Big\} + \xi_{ke}(\Delta x_k - \Delta x_j)\Big\{ \frac{V_0}{6} + F_{xe} - \frac{1}{6}\frac{d}{dt}\Delta x_j - \frac{\overline{v_x}}{6} \Big\} + \eta_{ke}(\Delta y_k - \Delta y_j)\Big\{ \frac{V_0}{6} + F_{xe} - \frac{1}{6}\frac{d}{dt}\Delta x_j - \frac{\overline{v_x}}{6} \Big\} \Bigg].$$

Because

$$\sum_k a_{ke}\Big\{ \frac{V_0}{6} + F_{xe} - \frac{\overline{v_x}}{6} \Big\} = 0$$

i.e.,

$$\Big(\frac{V_0}{6} + F_{xe} - \frac{\overline{v_x}}{6} \Big) = 0,$$

Eq. 34 becomes as

$$\frac{d^2}{dt^2}\Delta x_j = \sum_k \Bigg[a_{ke} \Big\{ A_k(\Delta x_k - \Delta x_j) + B_k(\Delta y_k - \Delta y_j) - \frac{1}{6}\frac{d}{dt}\Delta x_j \Big\} + \Big\{ \xi_{ke}(\Delta x_k - \Delta x_j) + \eta_{ke}(\Delta y_k - \Delta y_j) \Big\} \Big(-\frac{1}{6}\frac{d}{dt}\Delta x_j \Big) \Bigg]. \quad (36)$$

Using Eq. 32, and an approximation that ignores the second-order miniscule quantities, Eq. 35 can be transformed as follows:

$$\frac{d^2}{dt^2}\Delta y_j = \sum_k \Bigg[a_{ke} \Big\{ C_k(\Delta x_k - \Delta x_j) + D_k(\Delta y_k - \Delta y_j) - \frac{1}{6}\frac{d}{dt}\Delta y_j \Big\} + \Big\{ \xi_{ke}(\Delta x_k - \Delta x_j) + \eta_{ke}(\Delta y_k - \Delta y_j) \Big\} \Big(-\frac{1}{6}\frac{d}{dt}\Delta y_j \Big) \Bigg] \quad (37)$$

Eq. 36 and Eq. 37 are differential equations satisfied by a small disturbance.

Let us consider a longitudinal wave whose oscillation direction coincides with the wavenumber vector. The directions of arrival of the waves are γ and $\tan\gamma := p$. The oscillations of each component of (X_j, Y_j) are

$$\Delta x_j = e^{i(\theta(X_j+pY_j)-\omega t)} \tag{38}$$

$$\Delta y_j = p\Delta x_j \tag{39}$$

In contrast, the oscillation caused by a transverse wave arriving in the same direction is as follows:

$$\Delta x_j = e^{i(\theta(X_j+pY_j)-\omega t)} \tag{40}$$

$$\Delta y_j = -\frac{1}{p}\Delta x_j \tag{41}$$

Substituting Eq. 39 into Eq. 36 and Eq. 37, we obtain equations satisfied by the longitudinal components of the disturbance.

$$Eq.\ 36 \Leftrightarrow \frac{d^2}{dt^2}\Delta x_j = \sum_k \Bigg[a_{ke}\Big\{(A_k + pB_k)(\Delta x_k - \Delta x_j) - \frac{1}{6}\frac{d}{dt}\Delta x_j\Big\} + \Bigg\{(\xi_{ke} + p\eta_{ke})(\Delta x_k - \Delta x_j)\Big(-\frac{1}{6}\frac{d}{dt}\Delta x_j\Big)\Bigg\}\Bigg] \tag{42}$$

$$\frac{Eq.\ 37)}{p} \Leftrightarrow \frac{d^2}{dt^2}\Delta x_j = \sum_k \Bigg[a_{ke}\Big\{\Big(\frac{C_k}{p} + D_k\Big)(\Delta x_k - \Delta x_j) - \frac{1}{6}\frac{d}{dt}\Delta x_j\Big\} + \Bigg\{\big(\xi_{ke} + p\eta_{ke}\big)(\Delta x_k - \Delta x_j)\Big(-\frac{1}{6}\frac{d}{dt}\Delta x_j\Big)\Bigg\}\Bigg] \tag{43}$$

Subtracting Eq. 43 from Eq. 42, we obtain:

$$0 = \sum_k \Bigg[a_{ke}\Big\{(A_k + pB_k - \frac{C_k}{p} - D_k)(\Delta x_k - \Delta x_j)\Big\}\Bigg]. \tag{44}$$

Further, using Eq. 41 in Eq. 36 and Eq. 37, we obtain equations satisfied by the transverse wave component of the disturbance.

$$Eq.\ 36 \Leftrightarrow \frac{d^2}{dt^2}\Delta x_j = \sum_k \Bigg[a_{ke}\Big\{(A_k - \frac{B_k}{p})(\Delta x_k - \Delta x_j) - \frac{1}{6}\frac{d}{dt}\Delta x_j\Big\} + \Bigg\{(\xi_{ke} - \frac{\eta_{ke}}{p})(\Delta x_k - \Delta x_j)\Big(-\frac{1}{6}\frac{d}{dt}\Delta x_j\Big)\Bigg\}\Bigg] \tag{45}$$

$$-p\times Eq.\ 37 \Leftrightarrow \frac{d^2}{dt^2}\Delta x_j = \sum_k \left[a_{ke}\left\{ \left(-pC_k + D_k \right)(\Delta x_k - \Delta x_j) - \frac{1}{6}\frac{d}{dt}\Delta x_j \right\} \right.$$
$$\left. + \left\{ \left(\xi_{ke} - \frac{\eta_{ke}}{p} \right)(\Delta x_k - \Delta x_j)\left(-\frac{1}{6}\frac{d}{dt}\Delta x_j \right) \right\} \right] \quad (46)$$

Subtracting Eq. 46 from Eq. 45, we obtain

$$0 = \sum_k \left[a_{ke}\left\{ (A_k - \frac{B_k}{p} + pC_k - D_k)(\Delta x_k - \Delta x_j) \right\} \right]. \quad (47)$$

From the definition, $A_1 = A_2, \quad A_3 = A_4, \quad A_5 = A_6$. If the response time (or sensitivity) A_{ke} is also x-axis symmetric, $A_{1e} = A_{2e}, \quad A_{3e} = A_{4e}, \quad A_{5e} = A_{6e}$.

Considering a longitudinal wave arriving from $\gamma = 0^\circ \Leftrightarrow p = 0$, the following equation is obtained: $\Delta x_j = e^{i(\theta X_j - \omega t)} = e^{i\theta X_j} e^{-i\omega t}$, which we substitute into Eq. 42.

In the first section, using the wavy line in Eq. 42 yields

$$a_{1e}\{A_1(e^{i\theta X_1} - e^{i\theta X_j}) + \frac{i\omega}{6}e^{i\theta X_j}\}e^{-i\omega t}$$
$$+a_{2e}\{A_2(e^{i\theta X_2} - e^{i\theta X_j}) + \frac{i\omega}{6}e^{i\theta X_j}\}e^{-i\omega t}$$
$$+a_{3e}\{A_3(e^{i\theta X_3} - e^{i\theta X_j}) + \frac{i\omega}{6}e^{i\theta X_j}\}e^{-i\omega t}$$
$$+a_{4e}\{A_4(e^{i\theta X_4} - e^{i\theta X_j}) + \frac{i\omega}{6}e^{i\theta X_j}\}e^{-i\omega t}$$
$$+a_{5e}\{A_5(e^{i\theta X_5} - e^{i\theta X_j}) + \frac{i\omega}{6}e^{i\theta X_j}\}e^{-i\omega t}$$
$$+a_{6e}\{A_6(e^{i\theta X_6} - e^{i\theta X_j}) + \frac{i\omega}{6}e^{i\theta X_j}\}e^{-i\omega t}.$$

In addition, because the terms with a_{1e} and a_{2e}, and terms with a_{5e} and a_{6e} are the same, respectively, and $e^{i\theta X_3} - e^{i\theta X_j}$ and $e^{i\theta X_4} - e^{i\theta X_j}$ are zero, The first section, with the wavy line in Eq. 42 becomes

$$2a_{1e}\{A_1(e^{i\theta X_1} - e^{i\theta X_j}) + \frac{i\omega}{6}e^{i\theta X_j}\}e^{-i\omega t}$$
$$+2a_{5e}\{A_5(e^{i\theta X_5} - e^{i\theta X_j}) + \frac{i\omega}{6}e^{i\theta X_j}\}e^{-i\omega t}$$
$$+2a_{3e}\{\frac{i\omega}{6}e^{i\theta X_j}\}e^{-i\omega t}$$
$$= 2a_{1e}\{A_1(e^{i\theta(X_1 - X_j)} - 1) + \frac{i\omega}{6}\}e^{i\theta X_j}e^{-i\omega t}$$
$$+2a_{5e}\{A_5(e^{i\theta(X_5 - X_j)} - 1) + \frac{i\omega}{6}\}e^{i\theta X_j}e^{-i\omega t}$$

$$+2a_{3e}\{\frac{i\omega}{6}\}e^{i\theta X_j}e^{-i\omega t} \tag{48}$$

However, assuming $\xi_1 = \xi_2, \quad \xi_3 = \xi_4, \quad \xi_5 = \xi_6$ (symmetric a_k on the x-axis), the second section with the wavy line in Eq. 42 becomes

$$\begin{aligned}
&\xi_{1e}(\Delta x_1 - \Delta x_j)\frac{i\omega}{6}e^{i\theta X_j}e^{-i\omega t} \\
&+\xi_{2e}(\Delta x_2 - \Delta x_j)\frac{i\omega}{6}e^{i\theta X_j}e^{-i\omega t} \\
&+\xi_{3e}(\Delta x_3 - \Delta x_j)\frac{i\omega}{6}e^{i\theta X_j}e^{-i\omega t} \\
&+\xi_{4e}(\Delta x_4 - \Delta x_j)\frac{i\omega}{6}e^{i\theta X_j}e^{-i\omega t} \\
&+\xi_{5e}(\Delta x_5 - \Delta x_j)\frac{i\omega}{6}e^{i\theta X_j}e^{-i\omega t} \\
&+\xi_{6e}(\Delta x_6 - \Delta x_j)\frac{i\omega}{6}e^{i\theta X_j}e^{-i\omega t} \\
&= 2\xi_{1e}(\Delta x_1 - \Delta x_j)\frac{i\omega}{6}e^{i\theta X_j}e^{-i\omega t} \\
&+2\xi_{5e}(\Delta x_5 - \Delta x_j)\frac{i\omega}{6}e^{i\theta X_j}e^{-i\omega t} \\
&= 2\xi_{1e}(e^{i\theta(X_1 - X_j)} - 1)\frac{i\omega}{6}\left(e^{i\theta X_j}e^{-i\omega t}\right)^2 \\
&+2\xi_{5e}(e^{i\theta(X_5 - X_j)} - 1)\frac{i\omega}{6}\left(e^{i\theta X_j}e^{-i\omega t}\right)^2
\end{aligned} \tag{49}$$

Furthermore, the left side of Eq. 42 as follows:

$$-\omega^2 e^{i\theta X_j}e^{-i\omega t}. \tag{50}$$

From Eq. 48, Eq. 49, and Eq. 50, Eq. 42 is transformed by dividing both sides by $e^{i\theta X_j}e^{-i\omega t}$:

$$\begin{aligned}
-\omega^2 &= 2a_{1e}\{A_1(e^{i\theta(X_1 - X_j)} - 1) + \frac{i\omega}{6}\} \\
&+2a_{5e}\{A_5(e^{i\theta(X_5 - X_j)} - 1) + \frac{i\omega}{6}\} \\
&+2a_{3e}\frac{i\omega}{6} \\
&+2\xi_{1e}(e^{i\theta(X_1 - X_j)} - 1)\frac{i\omega}{6}e^{i(\theta X_j - \omega t)} \\
&+2\xi_{5e}(e^{i\theta(X_5 - X_j)} - 1)\frac{i\omega}{6}e^{i(\theta X_j - \omega t)}
\end{aligned} \tag{51}$$

Here, the terms with ξ_{1e} and ξ_{5e} are also second-order microquantities. Therefore,

$$-\omega^2 \approx 2a_{1e}\left[A_1(e^{i\theta(X_1-X_j)}-1)+\frac{i\omega}{6}\right]$$
$$+2a_{5e}\left[A_5(e^{i\theta(X_5-X_j)}-1)+\frac{i\omega}{6}\right]$$
$$+2a_{3e}\frac{i\omega}{6}.$$

Here, by defining $X_1-X_j=S, X_5-X_j=-S$, we obtain

$$-\omega^2 = 2a_{1e}\left[A_1(e^{i\theta S}-1)+\frac{i\omega}{6}\right]$$
$$+2a_{5e}\left[A_5(e^{i\theta S}-1)+\frac{i\omega}{6}\right]$$
$$+2a_{3e}\frac{i\omega}{6}. \tag{52}$$

Using Euler's formula, Eq. 52 becomes

$$\omega^2+-i\frac{a_{1e}+a_{3e}+a_{5e}}{3}\omega+(\cos(\theta S)-1)(2a_{1e}A_1+2a_{5e}A_5)+i\sin(\theta S)(2a_{1e}A_1-2a_{5e}A_5).$$

The quadratic formula yields the following solutions.

$$\omega = -\frac{i(a_{1e}+a_{3e}+a_{5e})}{6}$$
$$\pm\frac{1}{2}\sqrt{\frac{-(a_{1e}+a_{3e}+a_{5e})^2}{9}-4\{(\cos(\theta S)-1)(2a_{1e}A_1+2a_{5e}A_5)+i\sin(\theta S)(2a_{1e}A_1-2a_{5e}A_5)\}}$$
$$= -\frac{i(a_{1e}+a_{3e}+a_{5e})}{6}$$
$$\times\left[1\pm\sqrt{1+\frac{72}{(a_{1e}+a_{3e}+a_{5e})^2}\{(\cos(\theta S)-1)(a_{1e}A_1+a_{5e}A_5)+i\sin(\theta S)(a_{1e}A_1-a_{5e}A_5)\}}\right] \tag{53}$$

The amplitude of the wave is $e^{i(\vec{k}\cdot\vec{x}-\omega t)}$. Therefore, assuming $\omega=\alpha+i\beta$, the stable condition is $\beta=\mathrm{Im}(\omega)<0$. Now, because

$$\omega\div\left(-\frac{i(a_{1e}+a_{3e}+a_{5e})}{6}\right)=-\frac{6\beta}{(a_{1e}+a_{3e}+a_{5e})}+i\frac{6\alpha}{(a_{1e}+a_{3e}+a_{5e})},$$

the stable condition is

$$\beta=\mathrm{Im}(\omega)<0$$
$$\Leftrightarrow \mathrm{Real}\left(1\pm\sqrt{1+\frac{72}{(a_{1e}+a_{3e}+a_{5e})^2}\{(\cos(\theta S)-1)(a_{1e}A_1+a_{5e}A_5)+i\sin(\theta S)(a_{1e}A_1-a_{5e}A_5)\}}\right)>0$$

Let us define

$$1 \pm \sqrt{1 + \frac{72}{(a_{1e} + a_{3e} + a_{5e})^2}\{(\cos(\theta S) - 1)(a_{1e}A_1 + a_{5e}A_5) + i\sin(\theta S)(a_{1e}A_1 - a_{5e}A_5)\}} := a + ib,$$

$$1 + \frac{72}{(a_{1e} + a_{3e} + a_{5e})^2}\{(\cos(\theta S) - 1)(a_{1e}A_1 + a_{5e}A_5) := \rho, \text{ and}$$

$$\sin(\theta S)(a_{1e}A_1 - a_{5e}A_5) := \phi.$$

To obtain $a > 0$, $4(1-\rho) > \phi^2$ must be satisfied. Therefore,

$$-4\Omega(\cos(\theta S) - 1)(\widetilde{A_1} + \widetilde{A_5}) > \Omega^2 \sin^2(\theta S)(\widetilde{A_1} - \widetilde{A_5})^2$$

where

$$\Omega = \frac{72}{(a_{1e} + a_{3e} + a_{5e})^2}, \quad \widetilde{A_k} = a_{ke}A_k$$

should be satisfied. From this equation, we finally obtain a stable condition for longitudinal waves in the $p = 0$ direction.

$$4 > \Omega(1 + \cos(\theta S))\frac{(\widetilde{A_1} - \widetilde{A_5})^2}{(\widetilde{A_1} + \widetilde{A_5})}$$

$$\Leftrightarrow \frac{(a_{1e} + a_{3e} + a_{5e})^2}{18} > (1 + \cos(\theta S))\frac{(A_1 a_{1e} - A_5 a_{5e})^2}{A_1 a_{1e} + A_5 a_{5e}}.$$

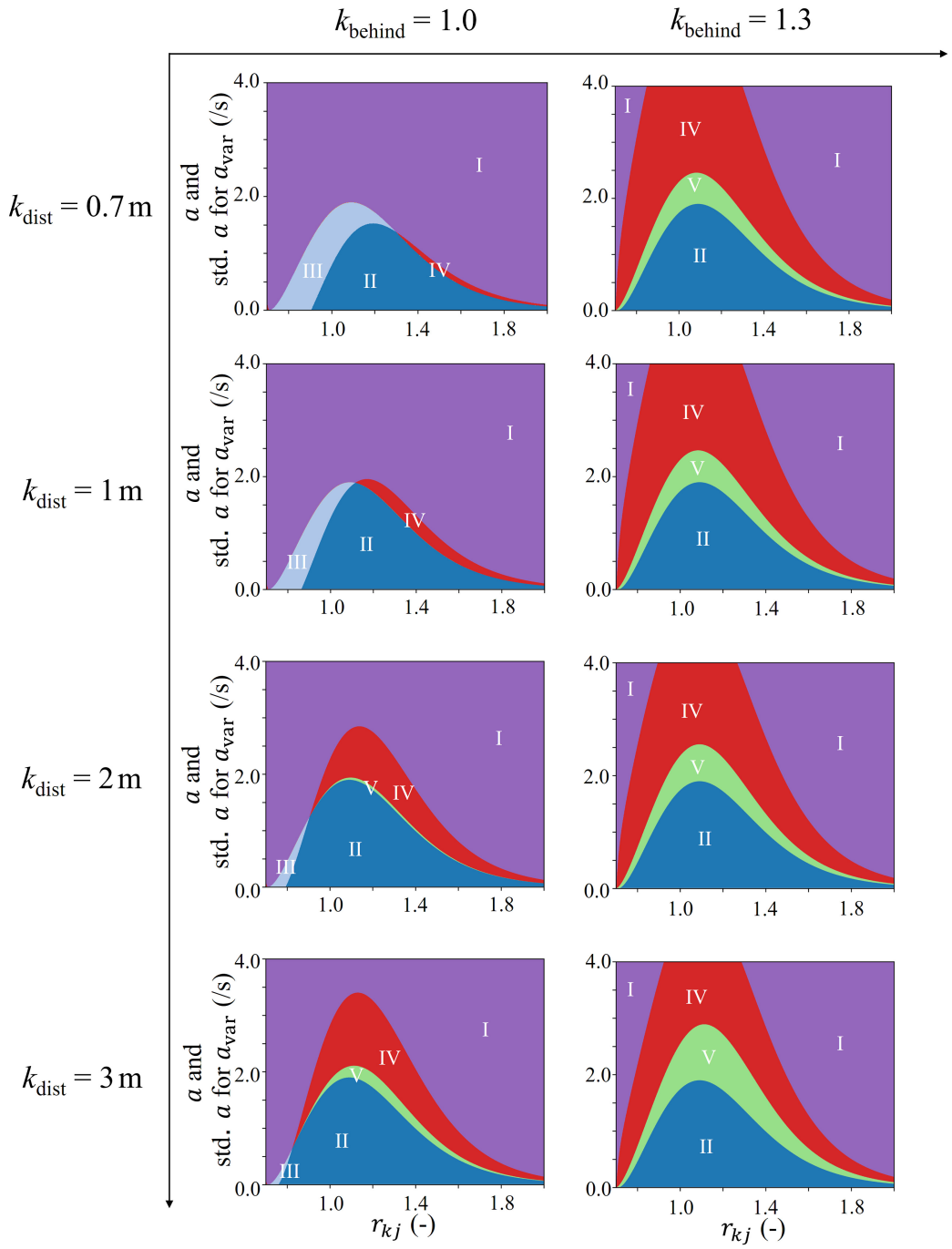

Figure 10 Sensitivity analysis on stability shift. Effects of k_{behind} and k_{dist} are evaluated.